

# Time Crystal in the Nonlinear Phonon Mode of the Trapped Ions

Yi-Ling Zhan,<sup>1</sup> Chun-Fu Liu,<sup>1</sup> J.-T. Bu,<sup>1</sup> K.-F Cui,<sup>1,\*</sup> S.-L. Su,<sup>1,2</sup> L.-L. Yan,<sup>1,2,†</sup> and Gang Chen<sup>1,‡</sup>

<sup>1</sup>*Key Laboratory of Materials Physics, Ministry of Education,  
School of Physics and Laboratory of Zhongyuan Light,  
Zhengzhou University, Zhengzhou 450001, China*

<sup>2</sup>*Institute of Quantum Materials and Physics, Henan Academy of Sciences, Zhengzhou 450046, China*

Time crystals constitute a novel phase of matter defined by the spontaneous breaking of time-translation symmetry. We present a scheme to realize a continuous-time crystal in the vibrational phonon mode of a trapped-ion system. By coupling two addressable traveling-wave lasers to the individual ions, we generate a nonlinear phonon mode with controllable linear gain and nonlinear damping via adiabatic elimination. This scheme enables stable dissipative dynamics over timescales significantly longer than the oscillation period, leading to the emergence of discrete time-translation symmetry breaking in the phonon mode, i.e., a phonon time crystal, under specific conditions. We further analyze the experimental feasibility and numerically demonstrate this phonon time crystal using accessible experimental parameters. These results provide a practical scheme for observing a time crystal in a nonlinear phonon mode, which will advance research into time crystals.

## I. INTRODUCTION

Time crystals, analogous to conventional spatial crystals, represent a many-body quantum state that spontaneously breaks time-translation symmetry in the ground state. Initially proposed by Wilczek and Shapere [1–3], this concept envisions a system capable of maintaining stable periodic motion without external energy input. However, theoretical studies reveal fundamental constraints: In classical systems with continuous symmetry, the ground state must remain static to prevent energy divergence, i.e., a principle termed as the "no-go" theorem [4–6]. Consequently, Wilczek's original model failed to satisfy thermodynamic equilibrium requirements [5].

The concept evolved from 2014 when Krzysztof Sacha introduce discrete time crystals (DTCs) within Floquet systems under periodic driving [7]. By applying an external field with period  $T$ , these systems exhibit subharmonic responses with integer periods  $nT (n > 1)$  [8], manifesting discrete time-translation symmetry breaking [9]. Notably, even with Hamiltonian perturbations, sufficient Ising interactions enable robust subharmonic responses [10]. Experimental breakthroughs began from 2017 with ion trap observations of period-doubling [11], followed by validations in nitrogen-vacancy centers and superconducting qubits [12–16].

By contrast, continuous time crystals (CTCs), which spontaneously form temporal periodicity without external driving [17–19], better align with Wilczek's original vision [2]. Their practical advantages in quantum technology spur research on dissipative time crystals [20–23]. In 2021, researchers first realize dissipative time crystals in a Bose-Einstein condensate coupled to an optical cavity [24], with subsequent demonstrations of CTCs in dissipative systems a year later [25, 26]. These researches

confirm the feasibility of circumventing the no-go theorem through environmental coupling to realize time crystal dynamics [27–31].

Recently, nonlinear systems with limit cycles prove to be a powerful platform for achieving this goal [32, 33]. By introducing linear damping, linear gain, and nonlinear damping, a feasible approach based on the nonlinear system is provided in [34], where the system exhibits a metastable state with stable oscillations during its time evolution, accompanied by a dissipative evolution process with a timescale far exceeding the oscillation period. If the dissipation processes can be precisely controlled in experiments, the time crystals can be observed.

As an ideal experimental platform, ion traps enable precise control and exhibit sophisticated engineering characteristics of dissipative mechanisms [35–40]. By tuning the detuning and Rabi frequencies of lasers, various gain and loss processes can be effectively produced, establishing ion traps as superb platforms for studying non-equilibrium and dissipative phenomena [41, 42]. Moreover, their precise single-ion addressing capability ensures the experimental accuracy and controllability of dissipative channels on different ions. Another significant advantage lies in high-fidelity fluorescence detection and quantum projection measurement techniques [43–47], which provide robust data support for investigating time crystal properties.

In this work, we demonstrate the experimental feasibility of realizing the continuous time crystal in the trapped ion system. The rest of this paper is organized as follows: In Sec. II, we choose the appropriate Hamiltonian and Lindblad operators to construct the required scheme for the realization of the time crystals in the trapped ion system. Subsequently, by using the adiabatic elimination method and removing high-frequency terms, we derive an effective Hamiltonian and effective Lindblad operators, which together form the effective Lindblad master equation of time crystals. In Sec. III, we perform a systematic analysis of the practically experimental parameters to validate the consistency of the theoretical scheme and its experimental feasibility. In Sec. IV, we use the feasi-

\* [cuikaifeng@zzu.edu.cn](mailto:cuikaifeng@zzu.edu.cn)

† [llyan@zzu.edu.cn](mailto:llyan@zzu.edu.cn)

‡ [chengang971@163.com](mailto:chengang971@163.com)

ble parameters to numerically solve the Lindblad master equation from a truncated Fock space, and demonstrate the characteristic behavior of time crystals: The system rapidly enters a metastable state with stable oscillations and subsequently evolves toward a steady state, with a decay time significantly longer than the oscillation period. In Sec. V, we discuss the impact of decoherence on time crystals, and the numerical simulation using a thermal state as the initial state has been performed and yields the similar results to those obtained when starting from a vacuum state, which thus demonstrates a remarkable robustness against decoherence of our continuous time crystal and ensures its sustained existence over extended periods. Finally, we give a brief conclusion in Sec. VI.

## II. MODEL OF THE SYSTEM

As shown in Fig. 1(a), we consider two  $^{40}\text{Ca}^+$  ions trapped in a linear ion trap, where the vibration of ions is driven by an external electric field with the amplitude  $E$  and frequency  $\omega_e$ . We combine two addressable traveling waves laser beams of 729 nm, one global 854 nm traveling laser with  $\sigma^+$  polarization, and a three-level system (see Fig. 1(b)) to produce different dissipative processes of vibrational phonon mode, where each of lasers serves a distinct purpose: The 854 nm laser is circularly polarized to produce a large effective dissipative process in the assistant two-level system, consisting of the ground state  $|0\rangle := |4^2S_{1/2}, m_s = -1/2\rangle$  and metastable state  $|1\rangle := |3^2D_{5/2}, m_s = -5/2\rangle$ , and these two addressed 729 nm lasers induce the linear gain ( $g$ ) and nonlinear damping ( $\kappa$ ), respectively, on the phonon mode.

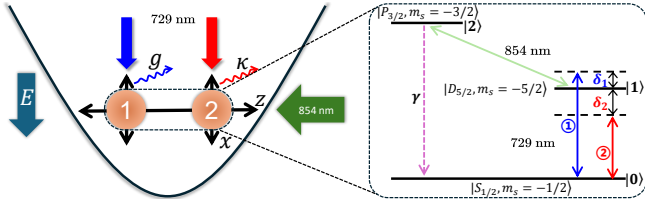


FIG. 1. The scheme to realize the time crystal in a trapped  $^{40}\text{Ca}^+$  ion system, where an external alternating electric field along the radial direction ( $x$ -direction) of ion is applied to drive the vibration of ion, an 854 nm laser couple the metastable state  $|1\rangle$  to the excited state  $|2\rangle := |4^2P_{3/2}, m_s = -3/2\rangle$  with the spontaneous emission rate  $\gamma$  to largely enhance the dissipation of  $|1\rangle$ , and two traveling wave laser beams of 729 nm with the detunings  $\delta_{1,2}$  couple the assistant system to the phonon mode to create the linear gain and nonlinear damping on the vibrational mode, respectively.

The Hamiltonian of the system can be divided into two parts: the vibrational mode Hamiltonian  $H_a$  and the spin states Hamiltonian  $H_s$ . For the vibrational mode, the Hamiltonian can be expressed as ( $\hbar = 1$ )

$$H_a = \omega_r a^\dagger a - 2qEx_0(a + a^\dagger) \cos(\omega_e t + \varphi) \quad (1)$$

where  $q$  is the elementary charge,  $a$  ( $a^\dagger$ ) represents the annihilation (creation) operators of radial center-of-mass vibrational phonon mode with the frequency  $\omega_r$ , the zero-point fluctuation  $x_0 = \sqrt{\hbar/4m\omega_r}$  with  $m$  denoting the mass of ion, and  $\varphi$  denotes the phase of electric field. In the interaction picture of  $\omega_e a^\dagger a$  and ignoring the high-frequency terms ( $e^{\pm 2\omega_e t}$ ), it reduced to  $H_a = -\Delta a^\dagger a + \varepsilon a^\dagger + \varepsilon^* a$  with the strength and detuning of electric field as  $\varepsilon = -2qEx_0 e^{-i\varphi}$  and  $\Delta = \omega_e - \omega_r$ .

The control process of spin states is also divided into two parts: the fast dissipative construction of a two-level system and the establishment of a nonlinear damping oscillator in the phonon mode. In the first part, we use the 854 nm laser to produce a dissipative two-level system in two ions that the Hamiltonian of two ions can be obtained as

$$H_1 = \frac{\Omega_e}{2} \sum_{n=1,2} (\tilde{\sigma}_{-,n} e^{i\omega_L^n t} + \text{h.c.}), \quad (2)$$

where the Pauli operators  $\tilde{\sigma}_{-,n} = |1\rangle_n \langle 2|$  for each ion, the Rabi frequency and frequency of 854 nm laser are  $\Omega_e$  and  $\omega_L^n$ , respectively. In the second part, two traveling waves of 729 nm laser beams with different frequencies severally couple the corresponding ion to the center-of-mass mode through the following Hamiltonian

$$H_2 = \sum_{n=1,2} \frac{\Omega_n}{2} \sin[\eta(a + a^\dagger) + \phi_n] (\sigma_{-,n} e^{i\omega_L^n t} + \text{h.c.}), \quad (3)$$

where the Pauli operators  $\sigma_{-,n} = |0\rangle_n \langle 1|$ , the Rabi frequencies, phases and frequencies of two traveling wave 729 nm laser beams are corresponding to  $\Omega_n = \bar{\Omega}_n/\sqrt{2}$ ,  $\phi_n$  and  $\omega_L^n$ . The Lamb-Dicke parameter is  $\eta = k \cos \alpha / \sqrt{4m\omega_r}$  with the laser wave vector  $k$  and projection angle  $\alpha$  between laser and the vibrational direction.

Rotating into the interaction picture of  $H_0 = \omega_e a^\dagger a + \sum_{n=1}^2 (\omega_1 |1\rangle_n \langle 1| + \omega_2 |2\rangle_n \langle 2|)$  with  $\omega_1$  ( $\omega_2$ ) denoting the energy of state  $|1\rangle$  ( $|2\rangle$ ), we can obtain the total Hamiltonian  $H_s = H_1 + H_2$  as

$$H_s = \sum_{n=1}^2 \left\{ \frac{\Omega_e}{2} \tilde{\sigma}_{-,n} e^{i\delta_e t} + \frac{\Omega_n}{2} \sin[\eta(a e^{-i\omega_e t} + a^\dagger e^{i\omega_e t}) + \phi_n] \sigma_{-,n} e^{i\delta_n t} + \text{h.c.} \right\}, \quad (4)$$

where the detunings of 729 nm lasers are corresponding to  $\delta_n = \omega_L^n - \omega_1$ , the detuning of 854 nm laser is set same to  $\delta_e = \omega_L^e + \omega_1 - \omega_2$  and the detuning of electric field is  $\Delta = \omega_e - \omega_r$ . To obtain a brief form of efficient decay rate, we set the 854 nm laser on resonance  $\delta_e = 0$  (i.e.,  $\omega_L^e = \omega_2 - \omega_1$ ).

The dynamics of the ions under the Markov approximation is described by the Lindblad master equation [48]:

$$\dot{\rho} = -i [H_s, \rho] + \frac{1}{2} \sum_{n=1}^2 (2L_n \rho L_n^\dagger - L_n^\dagger L_n \rho - \rho L_n^\dagger L_n), \quad (5)$$

where the quantum jump operator for the  $n$ th ion,  $L_n = \sqrt{\gamma}|0\rangle_n\langle 2|$ , describes decay from the excited state  $|2\rangle$  to the ground state  $|0\rangle$  with decay rate  $\gamma$ . We then apply two consecutive adiabatic elimination processes to generate linear gain and nonlinear damping in the phonon mode. First, we eliminate the excited state  $|2\rangle$  to obtain a large effective decay rate from the metastable state  $|1\rangle$  to  $|0\rangle$  (see Appendix A):

$$L_{\text{eff}} = \sum_{n=1}^2 i\sqrt{\Gamma}\sigma_{-,n}, \quad \Gamma = \frac{\Omega_e^2}{\gamma}, \quad (6)$$

where the conditions  $\gamma \gg \Omega_e \gg \Gamma$  need to be satisfied to ensure the adiabatic elimination of the state  $|2\rangle$ . Next, we adiabatically eliminate the metastable state  $|1\rangle$  to create the necessary dissipative/gain process on the vibrational mode by selecting the detunings and phases of 729 nm laser beams as  $\phi_1 = 0$  and  $\delta_1 = \omega_e$  for laser ①, and  $\phi_2 = \pi/2$  and  $\delta_2 = -2\omega_e$  for laser ②, respectively, to produce the linear and nonlinear coupling between the two-level system and the vibrational mode.

Since these two lasers are independent of each other, we first consider the first laser beam, which is given by

$$H_1 = \frac{\Omega_1}{2} \sin[\eta(ae^{i\omega_e t} + a^\dagger e^{i\omega_e t})](\sigma_{-,1}e^{i\delta_1 t} + \sigma_{+,1}e^{-i\delta_1 t}).$$

We set  $\Omega_1 \ll \omega_e$ , expand the sinusoidal function as a Taylor series, and neglect higher-order terms like  $e^{\pm 2i\omega_e t}, e^{\pm 3i\omega_e t}, \dots$ , obtaining

$$\sin[\eta(ae^{-i\omega_e t} + a^\dagger e^{i\omega_e t})] \simeq \tilde{\eta}_1(ae^{-i\omega_e t} + a^\dagger e^{i\omega_e t}), \quad (7)$$

where the effective Lamb-Dicke parameter of ions  $\tilde{\eta}_1 = \sum_{k=0}^{\infty} -\langle n \rangle^k \eta^{2k+1} C_{2k+1}^k / (2k+1)!$  with  $\langle n \rangle$  denoting the average phonon of vibrational mode and the binomial expansion coefficient  $C_{2k+1}^k = (2k+1)!/k!(k+1)!$ . Thus, the reduced Hamiltonian is rewritten as

$$H_1 = \frac{\tilde{\eta}_1 \Omega_1}{2} (a\sigma_{-,1} + a^\dagger \sigma_{+,1}). \quad (8)$$

Under the condition  $\Gamma \gg \tilde{\eta}_1 \Omega_1$ , the state  $|1\rangle$  of the first ion can be adiabatically eliminated, yielding the effective Hamiltonian of spin state  $H_1 = 0$  and dissipative operators on the phonon mode as

$$L_{1,\text{eff}} = -\frac{\tilde{\eta}_1 \Omega_1}{\sqrt{\Gamma}} a^\dagger |0\rangle_1 \langle 0|. \quad (9)$$

Then, we apply the same method to the second laser, where we have  $\cos[\eta(ae^{-i\omega_e t} + a^\dagger e^{i\omega_e t})] \simeq \tilde{\eta}_2(a^2 e^{-2i\omega_e t} + (a^\dagger)^2 e^{2i\omega_e t})$  where the effective Lamb-Dicke parameter  $\tilde{\eta}_2 = \sum_{k=1}^{\infty} -\langle n \rangle^{k-1} \eta^{2k} C_{2k}^{k-1} / (2k)!$ . Thus, we obtain the reduced Hamiltonian as

$$H_2 = \frac{\tilde{\eta}_2 \Omega_2}{2} [a^2 \sigma_{+,2} + (a^\dagger)^2 \sigma_{-,2}]. \quad (10)$$

Under the condition  $\Gamma \gg \tilde{\eta}_2 \Omega_2$ , the state  $|1\rangle$  of second ion can also be adiabatically eliminated, yielding the effective Hamiltonian of spin state  $H_2 = 0$  and dissipative operator as

$$L_{2,\text{eff}} = -\frac{\tilde{\eta}_2 \Omega_2}{\sqrt{\Gamma}} a^2 |0\rangle_2 \langle 0|. \quad (11)$$

By tracing over the spin state, the dynamics of phonon mode can be obtained as

$$\dot{\rho} = -i[H_a, \rho] + g\mathcal{D}[a^\dagger]\rho + \kappa\mathcal{D}[a^2]\rho, \quad (12)$$

where the superoperator  $\mathcal{D}[o]\rho = o\rho o^\dagger - (o^\dagger o\rho + \rho o^\dagger o)/2$ , the linear gain rate  $g = \tilde{\eta}_1^2 \Omega_1^2 / \Gamma$  and the nonlinear damping rate  $\kappa = \tilde{\eta}_2^2 \Omega_2^2 / \Gamma$ , respectively.

### III. EXPERIMENTAL FEASIBILITY

For the trapped  $^{40}\text{Ca}^+$  ion system, the life time of excited state  $4^2P_{3/2}$  is 6.9 ns, which gives a decay rate  $\gamma/2\pi = 22.4$  MHz [38]. The trap frequency is accessible in an interval  $\omega_t/2\pi \in [0.1, 10]$  MHz [49]. The 854 nm laser can drive a dipole transition between the metastable state and the excited state which produces a Rabi frequency of several MHz, even tens of MHz. The 729 nm laser drives a quadrupole transition between the metastable state and ground state. Its maximal Rabi frequency is generally around several hundred kHz and rarely reaches the MHz level [49]. Particularly, the Lamb-Dicke parameter of  $^{40}\text{Ca}^+$  is  $\eta \approx 0.1$  under a trap frequency of  $\omega_t/2\pi = 1$  MHz for a single ion. As the number of ions ( $N$ ) increases,  $\eta$  diminishes proportionally to  $1/\sqrt{N}$  due to the collective vibrational modes. Consequently, for the radial center-of-mass mode of two ions, the parameter ranges as  $\eta \in [0.022, 0.22]$  when the trap frequency is tuned within  $\omega_t/2\pi \in [0.1, 10]$  MHz to optimize ion coupling.

In the process of obtaining the linear gain and nonlinear damping processes on the vibrational mode, we have successively made different adiabatic approximations and neglect higher-order term, which restrict the involved parameters to satisfy the following chain relation

$$\gamma \gg \Omega_e, \omega_r \gg \Gamma \gg \tilde{\eta}_k \Omega_k \gg \varepsilon, \kappa, g \quad (13)$$

with  $k = 1, 2$ . Since the effective Lamb-Dicke parameter  $\tilde{\eta}_1 \propto \eta$ , the effective Rabi frequencies  $\tilde{\eta}_1 \Omega_1$  is general smaller than 50 kHz, meanwhile, the effective Rabi frequency  $\tilde{\eta}_2 \Omega_2$  is smaller than 5 kHz because of  $\tilde{\eta}_2 \propto \eta^2$ .

To simplify the process of demonstrating the time crystal of vibrational mode, we choose the frequency of radial center-of-mass mode as  $\omega_r/2\pi = 1$  MHz, giving the Lamb-Dicke parameter  $\eta = 0.07$ . The detuning of external electric field  $\Delta/2\pi = 5$  kHz, the Rabi frequency of 854 nm laser as  $\Omega_e/2\pi = 1.34$  MHz which gives an effective decay rate  $\Gamma/2\pi = 80$  kHz. In our scheme, we choose the vibrational ground state as the initial state for the evolution and obtain the approximate effective Lamb-Dicke parameters about  $\tilde{\eta}_1 \approx 0.066$  and  $\tilde{\eta}_2 \approx 0.0018$ . Then, the Rabi frequencies of the first 729 nm laser are chosen as  $\Omega_1/2\pi = 100$  kHz which produces  $g/2\pi = 0.54$  kHz. Besides, we explore the system's dynamics under different nonlinear damping rates by varying the Rabi frequency of the second laser  $\Omega_2$ .

## IV. PHONON TIME CRYSTAL OF VIBRATIONAL MODE

### A. Classical driven Van der Pol oscillator model

To further understand the dynamics of the quantum system, we first consider the dynamics in the thermodynamic limit that the Lindblad master equation can be further reduced to a driven classical Van der Pol oscillator model with the evolution of amplitude  $\alpha = \langle a \rangle$  described by the following differential equation (see Appendix B)

$$\dot{\alpha} = \left( \frac{g}{2} + i\Delta - \kappa|\alpha|^2 \right) \alpha - i\varepsilon. \quad (14)$$

It exhibits both the Hopf bifurcation and a limit cycle phase [50–53]. In the limit of  $\kappa \rightarrow 0$  [54], the Hopf bifurcation point can be characterized by the rescaled driving strength parameter  $\varepsilon\sqrt{\kappa} = \sqrt{g(g^2 + 4\Delta^2)/4}$ . This classical model is well studied and we focus on investigating the nonequilibrium behavior at the full quantum level, especially in the phonon mode of a quantum harmonic oscillator.

### B. Phonon time crystal of ions

To study the evolution of phonon number and purity, we numerically solve the time evolution of the vibrational mode in the Fock basis. In Fig. 2(a), we demonstrate the time evolution of the rescaled phonon number [55], defined as  $\Omega_2^2 N_a = \Omega_2^2 \langle a^\dagger a \rangle$ , for three distinct values of  $\Omega_2$ . With the decrease of  $\Omega_2$ , the associated nonlinear damping rate becomes weaker, resulting in two notable changes: an increase in the amplitude of oscillations and a lengthening of the relaxation time. These observations highlight the dynamic behavior of the system as it passes through different regimes. The oscillatory nature of the evolution provides the strong evidence for the dissipative gap closing in the thermodynamic limit, thereby confirming that the vibrational mode behaves as a time crystal. Besides, the time evolution approaches the classical situation with the decrease of  $\Omega_2$ .

In addition to examining the rescaled phonon number, as shown in Fig. 2(b), we also analyze the time-dependent evolution of the state purity that at the beginning of the evolution, the purity rapidly drops with the similar rate due to the system initially in the nonequilibrium state, and then the system enters a metastable state after this initial decrease, where the purity temporarily stabilizes before the following oscillations. Over time, the oscillations gradually dampen, and the system approaches a steady-state value of purity.

### C. Husimi $Q$ Function Analysis

To further depict the dynamics of time crystal, we study the evolution process of Husimi  $Q$  function defined as  $Q(\alpha) = \langle \alpha | \rho | \alpha \rangle / \pi$ , where  $|\alpha\rangle$  is a coherent state in

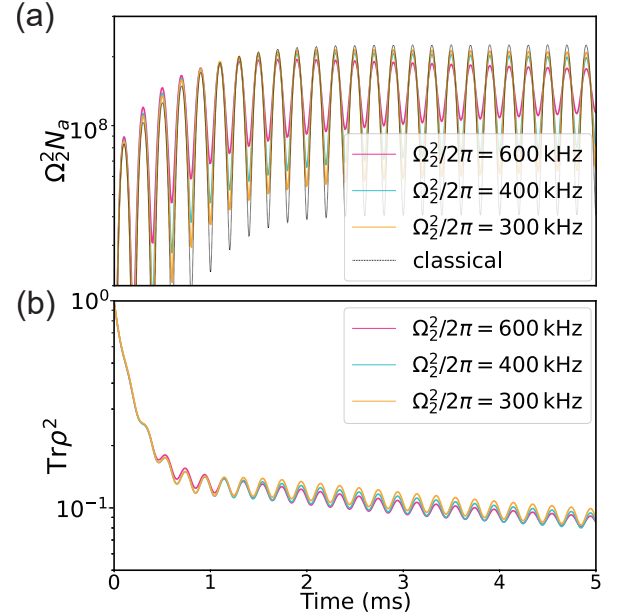


FIG. 2. The time evolution of (a) the rescaled phonon number  $\Omega_2^2 N_a$  and (b) the purity  $\text{Tr} \rho^2$ , where the black dashed line in panel (a) represents the time evolution of the classical mode with initial value of amplitude  $\alpha_0 = 0$ . The initial state of the vibrational mode is the vacuum state and the rescaled driving strength is chosen as  $\varepsilon\sqrt{\kappa} \approx \tilde{\eta}_2 \varepsilon \Omega_2 \sqrt{\gamma}/\Omega_e = 14.27 \text{ kHz}^{3/2}$ . Here, the other parameters are chosen by the accessible experimental parameters provided in the main text.

phase space with the complex number  $\alpha = q + ip$  corresponding to a specific point in the phase space [56]. The Husimi  $Q$  function provides a quasi-classical representation of the quantum state, allowing us to intuitively understand how the quantum state is distributed in the classical phase space. And it also provides a quasiprobability distribution and its maximal value can partially reflect the phase fluctuation of the quantum oscillation.

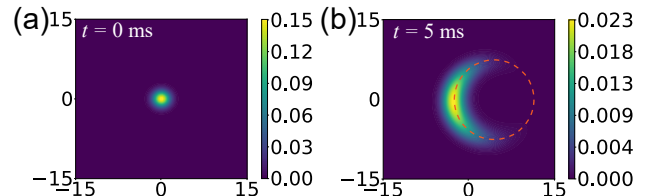


FIG. 3. Quantum Husimi distribution at  $t = 0$  (a) and  $t = 5$  ms (b), where the red dashed line represents the limit cycle and the Rabi frequency  $\Omega_2/2\pi = 300 \text{ kHz}$ .

Similar to the evolution of state purity, starting from the initial vacuum state, there is a rapid dephasing process at beginning, followed by a slowdown in the rate of dephasing, and then continuously oscillations [50]. Eventually, the oscillations gradually fade, and the quantum limit cycle becomes blurred. In Fig. 3(a) and 3(b), we illustrate the evolution of the  $Q$  function: Initially, the  $Q$  function appears as a Gaussian wave packet, reflecting the coherence of the initial state, which aligns with the

initial state of our setup, i.e., the vacuum state. As the evolution progresses, the  $Q$  function gradually disperses, where the wave packet rotates along the limit cycle in phase space and is increasingly elongated.

## V. ROBUST TO THE THERMAL EFFECT

In the practical experiments, the system cannot always be prepared in the vacuum state as described in Sec. IV or an ideal coherent state, but the state of the system more generally evolves into a thermal state with an effective temperature. Consequently, the impact of thermal effects on the evolution of the time crystal will be considered. Fortunately, our model demonstrates remarkable robustness against decoherence. As a result, we are able to directly use the thermal state as the initial condition. To discuss the thermal effect, we assume that we initially prepare the vibrational mode in a thermal state  $\rho_{\text{th}} = \exp(-\beta H_r)/\text{Tr}[\exp(-\beta H_r)]$  with the inverse temperature  $\beta = 1/k_B T$  ( $k_B$  is the Boltzmann constant and  $T$  is the effective temperature of vibrational state) and Hamiltonian of vibrational mode  $H_r = \hbar\omega_r a^\dagger a$  [57, 58]. This state gives an average phonon number  $\bar{n}_0 = \langle n \rangle = 1/(e^{\beta\hbar\omega_r} - 1)$  and a probability distribution on the Fock state  $|n\rangle$  as  $p_n = \bar{n}_0^n/(\bar{n}_0 + 1)^{n+1}$ .

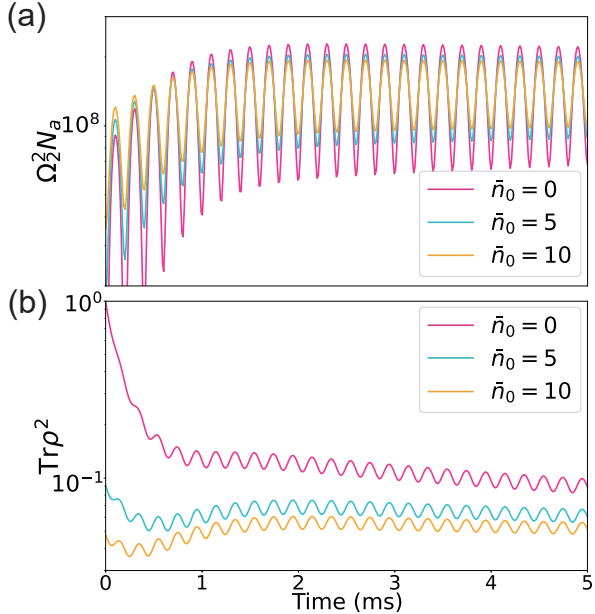


FIG. 4. The rescaled phonon number (a) and purity (b) for the evolution under different thermal states as the initial states, where  $\Omega_2/2\pi = 300$  kHz.

In Fig. 4, we discuss the evolution of the vibrational mode under three different thermal states that we first investigated the evolution of the rescaled phonon number, and show that the choice of the thermal state does not affect the oscillation period of the time crystal but only leads to changes in the amplitude. Due to the difficulty of measuring the phonon number distribution and

purity in practical experiments, we plot the evolution of the population in different Fock states and search for a simpler phenomenon to reveal the existence of time crystal. By selecting evolution times  $t$  between 2.5 ms and 3.75 ms, as shown in Fig. 5, we can clearly observe the oscillatory behaviour of the population in different Fock state. Besides, by using different thermal states as the initial state, the time crystals of phonon modes also show strong robustness against thermal effects that it is able to maintain their spontaneous breaking of time symmetry and enable them to persist for long periods of time. Thus, we can witness the time crystal by measuring the oscillatory behaviour of population evolution in a specific Fock, such as [15].

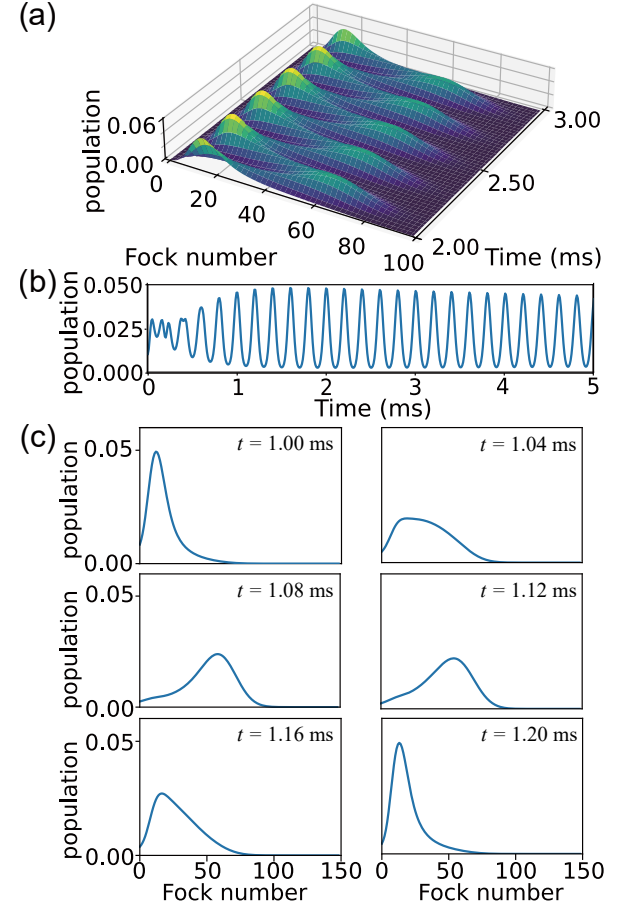


FIG. 5. The evolution of population in the Fock states for a initial thermal state with an average phonon  $\bar{n}_0 = 5$ . (a) The evolution of the population in different Fock states between 2.0 ms to 3.0 ms. (b) Evolution of the population in the Fock state  $|15\rangle$ . (c) The population in different Fock states at six equally time division points within the time range from  $t = 2.5$  ms to  $t = 2.75$  ms. Here, we also set  $\Omega_2/2\pi = 300$  kHz.

## VI. CONCLUSION

In summary, we have constructed a continuous-time crystal in a linear ion trap by employing two ions. Com-

pared to the existing methods for implementing discrete-time crystals in ion traps, our scheme offers enhanced stability for the time crystal behavior. Based on the practical parameters and detailed numerical simulations, we have verified the experimental feasibility of this scheme and observed the time-dependent evolution results for the system's phonon number, purity, and  $Q$ -function under ideal conditions, confirming the existence of the time crystal. Furthermore, through the use of different thermal states as initial conditions, we demonstrate that our continuous-time crystal model exhibits remarkable robustness against thermal effects, and also show that the oscillatory behaviour of population evolution in a specific Fock can be used as a simplified experimental method to witness the time crystal of phonon. Our findings provide a feasible approach for constructing time crystals and offer valuable insights for research in many-body physics and non-equilibrium thermodynamics.

## ACKNOWLEDGMENTS

This work is supported by the National Key Research and Development Program of China under Grant Nos. 2022YFA1404500 and 2021YFA1400902, by Cross-disciplinary Innovative Research Group Project of Henan Province under Grant No. 232300421004, National Natural Science Foundation of China under Grant Nos. 1232410, U21A20434, 12074346, 12274376, 12374466, 12074232, 12125406, by Natural Science Foundation of Henan Province under Grant Nos. 232300421075, 242300421212, by Major science and technology project of Henan Province under Grant No. 221100210400.

## Appendix A: Adiabatic Elimination of Spin States

The density matrix  $\rho$  of the system with the Hamiltonian  $H$  can be described by the Lindblad master equation as

$$\dot{\rho} = -i[H, \rho] + \frac{1}{2} \sum_{n=1}^2 [2L_n \rho L_n^\dagger - (L_n^\dagger L_n \rho + \rho L_n^\dagger L_n)],$$

with the dissipative operator  $L_n = \sqrt{\gamma}|0\rangle_n\langle 2|$ . Our aim is to reduce the system's dynamics to an effective master equation that only involves the vibrational mode. Thus, we use the effective operator formalism in Ref. [59] to adiabatic eliminate the spin of system, where the effective dynamics of methods can be described as

$$\dot{\rho} = -i[H_{\text{eff}}, \rho] + \frac{1}{2} \sum_{n=1}^2 \mathcal{D}[L_{n,\text{eff}}]\rho, \quad (\text{A1})$$

where the effective Hamiltonian and Lindblad operators are given as

$$H_{\text{eff}} = -\frac{1}{2}V_- [H_{\text{NH}}^{-1} + (H_{\text{NH}}^{-1})^\dagger] V_+ + H_g, \quad (\text{A2})$$

$$L_{n,\text{eff}}^k = L_n H_{\text{NH}}^{-1} V_+, \quad (\text{A3})$$

where  $V_+$  ( $V_-$ ) are the coupling terms between the excited-state subspace and ground-state subspace of system,  $H_g$  is the Hamiltonian of the ground-state subspace, and  $H_{\text{NH}}$  is the non-Hermitian Hamiltonian

$$H_{\text{NH}} = H_e - \frac{i}{2} \sum_k L_k^\dagger L_k, \quad (\text{A4})$$

with  $H_e$  being the Hamiltonian of the excited-state subspace. During this adiabatic elimination process, the dynamics of excited-state subspace should be much faster than the dynamics of ground-state subspace and the coupling dynamics between them, meanwhile, the coupling dynamics between them should be much faster than the dynamics of ground-state subspace.

We first eliminate the excited state  $|2\rangle$  of ions. In this situation, the original Hamiltonian are defined as  $H_R = H_a + H_g + H_e + V_- + V_+$  where the ground-state subspace Hamiltonian  $H_g = \sum_{n=1}^2 \Omega_n \{ \sin[\eta(ae^{-i\omega_e t} + a^\dagger e^{i\omega_e t}) + \phi_n] \sigma_{-,n} e^{i\delta_n t} + \text{h.c.} \}$ , the excited-state subspace Hamiltonian  $H_e = 0$ , the coupling terms between them  $V_- = \sum_{n=1}^2 \Omega_e \tilde{\sigma}_{-,n} / 2$  and  $V_+ = \sum_{n=1}^2 \Omega_e \tilde{\sigma}_{+,n} / 2$ , and the Lindblad operators  $L_n = \sqrt{\gamma}|0\rangle_n\langle 2|$ . Using Eq. (A4), we can obtain

$$H_{\text{NH}} = -\frac{i\gamma}{2} \sum_{n=1}^2 |2\rangle_n\langle 2|, \quad H_{\text{NH}}^{-1} = \frac{2i}{\gamma} \sum_{n=1}^2 |2\rangle_n\langle 2|, \quad (\text{A5})$$

which result into

$$H_{\text{eff}} = H_a + H_g, \quad L_{n,\text{eff}} = i \frac{\Omega_e}{\sqrt{\gamma}} \sigma_{-,n}, \quad (\text{A6})$$

giving an effective decay rate  $\Gamma = \Omega_e^2/\gamma$  from the metastable state  $|1\rangle$  to ground state  $|0\rangle$ . Moreover, the constraint conditions for adiabatic elimination mean that  $\gamma \gg \Omega_e \gg \Gamma, \Omega_n, \varepsilon$ .

Using the same method, we can then eliminate the metastable state  $|1\rangle$  to produce the necessary damping processes on the vibrational mode. In this adiabatic elimination process, we have

$$H_g = H_a, \quad H_e = 0, \quad (\text{A7})$$

$$V_+ = \frac{\tilde{\eta}_1 \Omega_1}{2} a^\dagger \sigma_{+,1} + \frac{\tilde{\eta}_2 \Omega_2}{2} a^2 \sigma_{+,2}, \quad (\text{A8})$$

$$V_- = \frac{\tilde{\eta}_1 \Omega_1}{2} a \sigma_{-,1} + \frac{\tilde{\eta}_2 \Omega_2}{2} (a^2)^\dagger \sigma_{-,2}, \quad (\text{A9})$$

which then give

$$H_{\text{NH}} = -\frac{i\Gamma}{2} \sum_{n=1}^2 |1\rangle_n\langle 1|, \quad H_{\text{NH}}^{-1} = \frac{2i}{\Gamma} \sum_{n=1}^2 |1\rangle_n\langle 1|. \quad (\text{A10})$$

Finally, it obtains

$$H_{\text{eff}} = H_a, \quad (A11)$$

$$L_{1,\text{eff}} = -\frac{\tilde{\eta}_1 \Omega_1}{\sqrt{\Gamma}} a^\dagger |0\rangle_1 \langle 0|, \quad L_{2,\text{eff}} = -\frac{\tilde{\eta}_2 \Omega_2}{\sqrt{\Gamma}} a^2 |0\rangle_2 \langle 0|,$$

which give the effective linear gain rate  $g = \tilde{\eta}_1^2 \Omega_1^2 / \Gamma$  and the effective nonlinear damp rate  $\kappa = \tilde{\eta}_2^2 \Omega_2^2 / \Gamma$ . Besides, the constraint conditions of adiabatic elimination can be obtained as  $\Gamma \gg \tilde{\eta}_1^2 \Omega_1, \tilde{\eta}_2^2 \Omega_2 \gg g, \kappa, \varepsilon$ .

## Appendix B: Classical Van der Pol model

For our purpose, we reduce the Lindblad master equation in Eq. (12) to the classical equation of the amplitude  $\alpha = \langle a \rangle$  in Eq. (14). To achieve this, we can right-multiply both sides of Eq. (12) by the annihilation oper-

ator  $a$  and then take the trace over it, obtaining

$$\begin{aligned} \text{Tr}\{\dot{\rho}a\} &= -i\text{Tr}\{[H_a, \rho]a\} \\ &\quad + \text{Tr}\{g\mathcal{D}[a^\dagger]\rho a\} + \text{Tr}\{\kappa\mathcal{D}[a^2]\rho a\}. \end{aligned} \quad (B1)$$

Substituting  $H_a = -\Delta a^\dagger a + \varepsilon a^\dagger + \varepsilon^* a$  into the above equation, we obtain

$$-\text{Tr}\{[H_a, \rho]a\} = \Delta\alpha - \varepsilon, \quad (B2)$$

where we use the relation  $a^\dagger a = aa^\dagger - 1$  and the cyclic property of the trace. Similarly, the gain and damping terms  $\text{Tr}\{g\mathcal{D}[a^\dagger]\rho a\}$  and  $\text{Tr}\{\kappa\mathcal{D}[a^2]\rho a\}$  can be obtained as

$$\begin{aligned} \text{Tr}\{g\mathcal{D}[a^\dagger]\rho a\} &= \frac{g}{2} \text{Tr}\{\rho a^2 a^\dagger - \rho a a^\dagger a\} = \frac{g}{2}\alpha, \\ \text{Tr}\{\kappa\mathcal{D}[a^2]\rho a\} &= \frac{\lambda}{2} \text{Tr}[\rho(a^\dagger)^2 a^3 - \rho a(a^\dagger)^2 a^2] = -\lambda|\alpha|^2\alpha. \end{aligned} \quad (B3)$$

Consequently, we arrive at the following expression:

$$\dot{\alpha} = \left( \frac{g - \kappa}{2} + i\Delta \right) \alpha - \lambda|\alpha|^2\alpha - i\varepsilon, \quad (B4)$$

where  $\varepsilon\sqrt{\lambda}$  is a constant.

---

[1] A. Shapere and F. Wilczek, Classical time crystals, *Phys. Rev. Lett.* **109**, 160402 (2012).

[2] F. Wilczek, Quantum time crystals, *Phys. Rev. Lett.* **109**, 160401 (2012).

[3] F. Wilczek, Superfluidity and space-time translation symmetry breaking, *Phys. Rev. Lett.* **111**, 250402 (2013).

[4] P. Bruno, Comment on “quantum time crystals”, *Phys. Rev. Lett.* **110**, 118901 (2013).

[5] P. Bruno, Impossibility of spontaneously rotating time crystals: A no-go theorem, *Phys. Rev. Lett.* **111**, 070402 (2013).

[6] H. Watanabe and M. Oshikawa, Absence of quantum time crystals, *Phys. Rev. Lett.* **114**, 251603 (2015).

[7] K. Sacha, Modeling spontaneous breaking of time-translation symmetry, *Phys. Rev. A* **91**, 033617 (2015).

[8] V. Khemani, A. Lazarides, R. Moessner, and S. L. Sondhi, Phase structure of driven quantum systems, *Phys. Rev. Lett.* **116**, 250401 (2016).

[9] D. V. Else, C. Monroe, C. Nayak, and N. Y. Yao, Discrete time crystals, *Annu. Rev. Condens. Matter Phys.* **11**, 467 (2020).

[10] N. Y. Yao, A. C. Potter, I.-D. Potirniche, and A. Vishwanath, Discrete time crystals: Rigidity, criticality, and realizations, *Phys. Rev. Lett.* **118**, 030401 (2017).

[11] H. P. W. Zhang, J. A. Kyprianidis, P. Becker, A. Lee, J. Smith, G. Pagano, I.-D. Potirniche, A. C. Potter, A. Vishwanath, N. Y. Yao, and C. Monroe, Observation of a discrete time crystal, *Nature* **543**, 217 (2017).

[12] S. Choi, J. Choi, R. Landig, G. Kucska, H. Zhou, J. Isoya, F. Jelezko, S. Onoda, H. Sumiya, V. Khemani, C. von Keyserlingk, N. Y. Yao, E. Demler, and M. D. Lukin, Observation of discrete time-crystalline order in a disordered dipolar many-body system, *Nature* **543**, 221 (2017).

[13] W. W. Ho, S. Choi, M. D. Lukin, and D. A. Abanin, Critical time crystals in dipolar systems, *Phys. Rev. Lett.* **119**, 010602 (2017).

[14] X. Mi, M. Ippoliti, C. Quintana, A. Greene, Z. Chen, J. Gross, F. Arute, K. Arya, J. Atalaya, R. Babbush, J. C. Bardin, J. Basso, A. Bengtsson, A. Bilmes, A. Bourassa, L. Brill, M. Broughton, B. B. Buckley, D. A. Buell, B. Burkett, N. Bushnell, B. Chiaro, R. Collins, W. Courtney, D. Debroy, S. Demura, A. R. Derk, A. Dunsworth, D. Eppens, C. Erickson, E. Farhi, A. G. Fowler, B. Foxen, C. Gidney, M. Giustina, M. P. Harrigan, S. D. Harrington, J. Hilton, A. Ho, S. Hong, T. Huang, A. Huff, W. J. Huggins, L. B. Ioffe, S. V. Isakov, J. Iveland, E. Jeffrey, Z. Jiang, C. Jones, D. Kafri, T. Khattar, S. Kim, A. Kitaev, P. V. Klimov, A. N. Korotkov, F. Kostritsa, D. Landhuis, P. Laptev, J. Lee, K. Lee, A. Locharla, E. Lucero, O. Martin, J. R. McClean, T. McCourt, M. McEwen, K. C. Miao, M. Mohseni, S. Montazeri, W. Mruczkiewicz, O. Naaman, M. Neeley, C. Neill, M. Newman, M. Y. Niu, T. E. O’Brien, A. Opremcak, E. Ostby, B. Pato, A. Petukhov, N. C. Rubin, D. Sank, K. J. Satzinger, V. Shvarts, Y. Su, D. Strain, M. Szalay, M. D. Trevithick, B. Villalonga, T. White, Z. J. Yao, P. Yeh, J. Yoo, A. Zalcman, H. Neven, S. Boixo, V. Smelyanskiy, A. Megrant, J. Kelly, Y. Chen, S. L. Sondhi, R. Moessner, K. Kechedzhi, V. Khemani, and P. Roushan, Time-crystalline eigenstate order on a quantum processor, *Nature* **601**, 531 (2022).

[15] P. Frey and S. Rachel, Realization of a discrete time crystal on 57 qubits of a quantum computer, *Science Advances* **8**, eabm7652 (2022).

[16] H. Wang, Y.-J. Zhao, H.-C. Sun, X.-W. Xu, Y. Li, Y. Zheng, Q. Liu, and R. Li, Controlling the qubit-qubit

coupling in the superconducting circuit with double-resonator couplers, *Phys. Rev. A* **109**, 012601 (2024).

[17] V. K. Kozin and O. Kyriienko, Quantum time crystals from hamiltonians with long-range interactions, *Phys. Rev. Lett.* **123**, 210602 (2019).

[18] A. Greilich, N. E. Kopteva, A. N. Kamenskii, P. S. Sokolov, V. L. Korenev, and M. Bayer, Robust continuous time crystal in an electron-nuclear spin system, *Nat. Phys.* **20**, 631 (2024).

[19] N. I. Zheludev and K. F. MacDonald, Realization of a continuous time crystal in a photonic metamaterial, *Nat. Phys.* **19**, 939 (2023).

[20] F. Iemini, A. Russomanno, J. Keeling, M. Schirò, M. Dalmonte, and R. Fazio, Boundary time crystals, *Phys. Rev. Lett.* **121**, 035301 (2018).

[21] Z. Gong, R. Hamazaki, and M. Ueda, Discrete time-crystalline order in cavity and circuit qed systems, *Phys. Rev. Lett.* **120**, 040404 (2018).

[22] F. M. Gambetta, F. Carollo, M. Marcuzzi, J. P. Garrahan, and I. Lesanovsky, Discrete time crystals in the absence of manifest symmetries or disorder in open quantum systems, *Phys. Rev. Lett.* **122**, 015701 (2019).

[23] B. Buća and D. Jaksch, Dissipation induced nonstationarity in a quantum gas, *Phys. Rev. Lett.* **123**, 260401 (2019).

[24] H. Keßler, P. Kongkhambut, C. Georges, L. Mathey, J. G. Cosme, and A. Hemmerich, Observation of a dissipative time crystal, *Phys. Rev. Lett.* **127**, 043602 (2021).

[25] P. Kongkhambut, J. Skulte, L. Mathey, J. G. Cosme, A. Hemmerich, and H. Keßler, Observation of a continuous time crystal, *Science* **377**, 670 (2022).

[26] L. J. LeBlanc, Unleashing spontaneity in a time crystal, *Science* **377**, 576 (2022).

[27] Y.-X. Xiang, Q.-L. Lei, Z. Bai, and Y.-Q. Ma, Self-organized time crystal in driven-dissipative quantum system, *Phys. Rev. Res.* **6**, 033185 (2024).

[28] D. Chen, Z. Peng, J. Li, S. Chesi, and Y. Wang, Discrete time crystal in an open optomechanical system, *Phys. Rev. Res.* **6**, 013130 (2024).

[29] A. Riera-Campeny, M. Moreno-Cardoner, and A. Sanpera, Time crystallinity in open quantum systems, *Quantum* **4**, 270 (2020).

[30] B. Das, N. Jaseem, and V. Mukherjee, Discrete time crystals in the presence of non-markovian dynamics, *Phys. Rev. A* **110**, 012208 (2024).

[31] A. Lazarides, S. Roy, F. Piazza, and R. Moessner, Time crystallinity in dissipative floquet systems, *Phys. Rev. Res.* **2**, 022002 (2020).

[32] M. Krishna, P. Solanki, M. Hajdušek, and S. Vinjanampathy, Measurement-induced continuous time crystals, *Phys. Rev. Lett.* **130**, 150401 (2023).

[33] X. Wu, Z. Wang, F. Yang, R. Gao, C. Liang, M. K. Tey, X. Li, T. Pohl, and L. You, Dissipative time crystal in a strongly interacting rydberg gas, *Nat. Phys.* **20**, 1389 (2024).

[34] Y. Li, C. Wang, Y. Tang, and Y.-C. Liu, Time crystal in a single-mode nonlinear cavity, *Phys. Rev. Lett.* **132**, 183803 (2024).

[35] A. Bermudez, T. Schaetz, and M. B. Plenio, Dissipation-assisted quantum information processing with trapped ions, *Phys. Rev. Lett.* **110**, 110502 (2013).

[36] X.-Q. Shao, Engineering steady entanglement for trapped ions at finite temperature by dissipation, *Phys. Rev. A* **98**, 042310 (2018).

[37] D. C. Cole, J. J. Wu, S. D. Erickson, P.-Y. Hou, A. C. Wilson, D. Leibfried, and F. Reiter, Dissipative preparation of w states in trapped ion systems, *New J. Phys.* **23**, 073001 (2021).

[38] L.-L. Yan, J.-W. Zhang, M.-R. Yun, J.-C. Li, G.-Y. Ding, J.-F. Wei, J.-T. Bu, B. Wang, L. Chen, S.-L. Su, F. Zhou, Y. Jia, E.-J. Liang, and M. Feng, Experimental verification of dissipation-time uncertainty relation, *Phys. Rev. Lett.* **128**, 050603 (2022).

[39] T. Behrle, T. L. Nguyen, F. Reiter, D. Baur, B. de Neeve, M. Stadler, M. Marinelli, F. Lancellotti, S. F. Yelin, and J. P. Home, Phonon laser in the quantum regime, *Phys. Rev. Lett.* **131**, 043605 (2023).

[40] L.-L. Yan, J.-T. Bu, Q. Zeng, K. Zhang, K.-F. Cui, F. Zhou, S.-L. Su, L. Chen, J. Wang, G. Chen, and M. Feng, Experimental verification of demon-involved fluctuation theorems, *Phys. Rev. Lett.* **133**, 090402 (2024).

[41] H. C. Nägerl, D. Leibfried, H. Rohde, G. Thalhammer, J. Eschner, F. Schmidt-Kaler, and R. Blatt, Laser addressing of individual ions in a linear ion trap, *Phys. Rev. A* **60**, 145 (1999).

[42] S. Charles Doret, J. M. Amini, K. Wright, C. Volin, T. Killian, A. Ozakin, D. Denison, H. Hayden, C.-S. Pai, R. E. Slusher, and A. W. Harter, Controlling trapping potentials and stray electric fields in a microfabricated ion trap through design and compensation, *New J. Phys.* **14**, 073012 (2012).

[43] W. J. Setzer, M. Ivory, O. Slobodyan, J. W. Van Der Wall, L. P. Parazzoli, D. Stick, M. Gehl, M. G. Blain, R. R. Kay, and H. J. McGuinness, Fluorescence detection of a trapped ion with a monolithically integrated single-photon-counting avalanche diode, *Appl. Phys. Lett.* **119**, 154002 (2021).

[44] P. Schindler, D. Nigg, T. Monz, J. T. Barreiro, E. Martinez, S. X. Wang, S. Quint, M. F. Brandl, V. Nebendahl, C. F. Roos, M. Chwalla, M. Hennrich, and R. Blatt, A quantum information processor with trapped ions, *New J. Phys.* **15**, 123012 (2013).

[45] K. Okada, M. Wada, T. Nakamura, T. Takayanagi, I. Katayama, and S. Ohtani, Space-charge shift in motional resonance of ca+ induced by simultaneously trapped molecular ions in linear paul trap, *Jpn. J. Appl. Phys.* **45**, 951 (2006).

[46] Z. Fei, X. Yi, X. You-Yang, L. Jiao-Mei, H. Xue-Ren, and F. Mang, Control of a cloud of laser-cooled 40ca+ in a linear ion trap, *Chin. Phys. Lett.* **27**, 043201 (2010).

[47] S. Ding, G. Maslennikov, R. Hablützel, and D. Matsukevich, Cross-kerr nonlinearity for phonon counting, *Phys. Rev. Lett.* **119**, 193602 (2017).

[48] G. Lindblad, On the generators of quantum dynamical semigroups, *Commun. Math. Phys.* **48**, 119 (1976).

[49] C. Monroe, W. C. Campbell, L.-M. Duan, Z.-X. Gong, A. V. Gorshkov, P. W. Hess, R. Islam, K. Kim, N. M. Linke, G. Pagano, P. Richerme, C. Senko, and N. Y. Yao, Programmable quantum simulations of spin systems with trapped ions, *Rev. Mod. Phys.* **93**, 025001 (2021).

[50] C. Navarrete-Benlloch, T. Weiss, S. Walter, and G. J. de Valcárcel, General linearized theory of quantum fluctuations around arbitrary limit cycles, *Phys. Rev. Lett.* **119**, 133601 (2017).

[51] L. Ben Arosh, M. C. Cross, and R. Lifshitz, Quantum limit cycles and the rayleigh and van der pol oscillators, *Phys. Rev. Res.* **3**, 013130 (2021).

- [52] T. Weiss, S. Walter, and F. Marquardt, Quantum-coherent phase oscillations in synchronization, *Phys. Rev. A* **95**, 041802 (2017).
- [53] S. Sonar, M. Hajdušek, M. Mukherjee, R. Fazio, V. Vedral, S. Vinjanampathy, and L.-C. Kwek, Squeezing enhances quantum synchronization, *Phys. Rev. Lett.* **120**, 163601 (2018).
- [54] W. Casteels, R. Fazio, and C. Ciuti, Critical dynamical properties of a first-order dissipative phase transition, *Phys. Rev. A* **95**, 012128 (2017).
- [55] J. Johansson, P. Nation, and F. Nori, Qutip: An open-source python framework for the dynamics of open quantum systems, *Comput. Phys. Commun.* **183**, 1760 (2012).
- [56] K. Husimi, Some formal properties of the density matrix, *Proc. Phys. Math. Soc.* **22**, 264 (1940).
- [57] F. Strocchi, Thermal states, in *Symmetry Breaking* (Springer Berlin Heidelberg, Berlin, Heidelberg, 2008) pp. 139–150.
- [58] Y. Guryanova, S. Popescu, A. J. Short, R. Silva, and P. Skrzypczyk, Thermodynamics of quantum systems with multiple conserved quantities, *Nat. Commun* **7**, 12049 (2016).
- [59] F. Reiter and A. S. Sørensen, Effective operator formalism for open quantum systems, *Phys. Rev. A* **85**, 032111 (2012).